Research Article
Vol. 31, No. 19 / 11 Sep 2023 / Optics Express 31300
Optics EXPRESS

Monolithic integrated all-GaN-based µLED display by selective area regrowth

YAYING LIU,[1,2] ZHAOJUN LIU,[1,3] AND KEI MAY LAU[2,4]

[1] Department of Electrical and Electronic Engineering, Southern University of Science and Technology, Shenzhen 518055, China
[2] Department of Electronic and Computer Engineering, The Hong Kong University of Science and Technology, Clear Water Bay, Hong Kong, China
[3] liuzj@sustech.edu.cn
[4] eekmlau@ust.hk

Abstract: This work demonstrates an all-GaN-based µLED display with monolithic integrated HEMT and µLED pixels using the selective area regrowth method. The monochrome µLED-HEMT display has a resolution of 20×20 and a pixel pitch of 80 µm. With the optimized regrowth pattern, the µLED-HEMT achieves a maximum light output power of 36.2 W/cm^2 and a peak EQE of 3.36%, mainly due to the improved crystal quality of regrown µLED. TMAH treatment and Al_2O_3 surface passivation are also performed to minimize the impact of nonradiative recombination caused by the dry etching damage. With a custom-designed driving circuit board, images of "HKUST" are successfully shown on the µLED-HEMT display.

© 2023 Optica Publishing Group under the terms of the Optica Open Access Publishing Agreement

1. Introduction

GaN-based µLED displays have attracted considerable attention as a promising candidate for AR/VR, head-up display, and high-resolution TV due to their superior optical and physical properties such as self-emissive, high luminance, wide color gamut, and long lifespan [1–3]. Active-matrix driving mode is usually adopted for µLED display, in which µLED pixels are driven individually and could remain lit up during a whole frame. Like LCD and OLED displays, the individual control of the µLED pixels is achieved by the pixel driving circuit built from thin film transistors (TFTs) or Si-based complementary metal-oxide-semiconductor transistors (CMOS). Due to the different semiconductor materials of µLEDs and pixel circuits, the realization of µLED displays requires additional integration processes for separately fabricated µLED arrays and driver chips, such as wafer bonding, flip-chip bonding (FCB) and pick-and-place technologies [4,5]. In these integration techniques, precise alignment and placement are big challenges with millions of pixels in the display. With the increase of pixel density and shrink of pixel size, the difficulties in achieving high yield and high precision integration through hybrid integration processes increase aggressively, hindering the realization of low-cost, large-scale manufacturing. In addition, in the bonding process, due to the thermal expansion mismatch between GaN and Si materials, the built-in stress between the µLED array and driver chip will result in bonding failure and affect the long-term reliability of the display system [6]. Therefore, homogeneous and monolithic integration of µLED and GaN-based driving circuits has been considered one of the solutions, i.e.,µLEDs and driving circuits fabricated on the same epitaxial wafer without additional assembly processes. The monolithic integration of LED and GaN-based high electron mobility transistors (HEMTs), MOSFETs, and nanowire FETs have been reported [7–11].

HEMT has electron mobility over 2000 cm^2/V·s due to two-dimensional electron gas (2DEG) [12]. Therefore, as the driving transistor for µLED, a smaller device dimension is required for a specific driving current, which is conducive to achieving a smaller pixel size. The low on-resistance of HEMT is also beneficial to achieving low-power displays, which is essential for wearable and portable devices for which long battery life is more favored [13]. C Liu et al. have

#502275
Journal © 2023
https://doi.org/10.1364/OE.502275
Received 2 Aug 2023; revised 21 Aug 2023; accepted 24 Aug 2023; published 6 Sep 2023

reported a metal-interconnection-free HEMT-LED device with a standard LED size using the selective area regrowth (SAR) method [14]. LED epitaxial layers are selectively regrown on a selectively etched HEMT wafer, resulting in monolithic integration by connecting HEMT and LED laterally without additional metal connection. In this integration scheme, the resistance of HEMT-LED is further reduced by eliminating the parasitic resistance induced by the metal wire that connects the LED and HEMT, leading to a more energy-efficient integration scheme.

However, a big challenge in using SAR to achieve μLED display is regrown μLEDs with high crystal quality, ensuring a high luminance and quantum efficiency. Y Cai et al. have demonstrated an 8×8 μLEDs/HEMTs microdisplay by a direct selective regrown method [15]. In their work, to avoid etching damages on the μLEDs sidewall, μLED pixels are directly formed in periodically arranged micro holes by SAR without additional dry etching. The light output power (LOP) of the μLEDs/HEMT is 10 W/cm^2 at a current density of ~7000 A/cm^2. The low LOP could originate from the poor crystal quality of regrown μLED. Different from conventional planar epitaxial growth, using of regrowth mask in the SAR process induces the accumulation of source materials above the mask region. The additional sources would laterally diffuse to the regrowth window driven by the concentration gradient, known as lateral vapor-phase diffusion (LVD), leading to extra sources reaching the regrowth region. Another path of the extra sources is to adsorb and then migrate from the mask region (MMR) to the regrowth window [16]. The additional sources will enhance the growth rate, especially at the edge of the regrowth window, resulting in a faster and nonuniform growth rate in the regrowth window. The nonuniformly distributed sources will also aggravate the alloy composition nonuniformity in InGaN/GaN MQWs [17]. As a result, it becomes harder to regrow homogenous MQWs with high crystal quality in the SAR process. Moreover, lateral overgrowth happens simultaneously with vertical growth, which makes the regrown LED exceed the regrowth window and form an undesired epitaxial structure above the regrowth mask [18]. Further, the regrowth mask could introduce impurities to the regrown μLED, creating nonradiative recombination centers and degrading the performance of μLED [19,20].

Obtaining high-quality regrown μLED in integrating HEMTs and GaN-based μLED becomes crucial in using the SAR method. It has been reported that the morphology and quality of the selective regrown epitaxial structure could be affected by the geometry and arrangement of the regrowth mask. A. Tanaka et al. investigated the effect of mask geometry on selective area growth. It was reported that the increment in growth rate could be alleviated with large growth windows and small spacing between the windows [21]. Selective growth with a small mask region can mitigate the inhomogeneity of component composition in MQWs from the edge to the center of the growth window [17]. Besides, M Ueta et al. showed that QWs selectively grown with a large window and small mask region have a similar photoluminescence (PL) spectrum as the planar-grown QWs, while the QWs grown with a small window and large mask region form PL emission from $(11\bar{2}2)$ facet [22]. These findings motivate us to design a regrowth pattern with a large window ratio for μLED regrowth, which is expected to significantly improve the

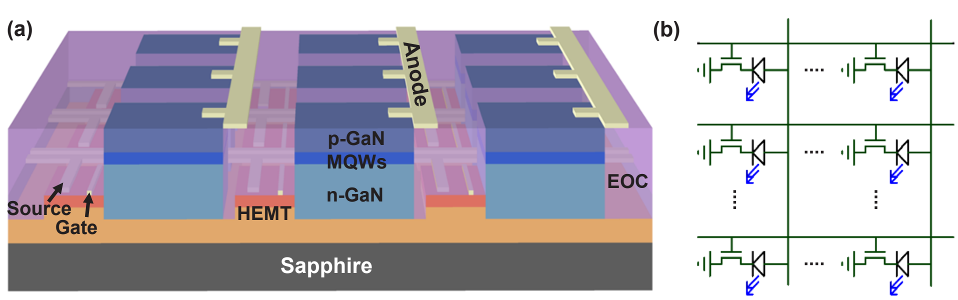

Fig. 1. (a) Schematic diagram and (b) equivalent circuit of the μLED-HEMT display

performance of the µLED device with improved crystal quality. The window ratio is defined by the proportion of the regrowth window to the whole area. In this work, we present the enhanced device performance of a µLED-HEMT display with a 50 µm µLED and 80 µm pixel pitch by using the optimized regrowth pattern. Our approach results in a maximum LOP density of 36.2 W/cm^2 at 620 A/cm^2 and a peak EQE of 3.36%. Figure 1 shows the schematic diagram and equivalent circuit of the µLED-HEMT display.

2. Experiments

Figure 2 illustrates the details of the SAR process for the µLED-HEMT display. A commercial 2-inch AlGaN/GaN HEMT epitaxial wafer grown by Enkris Inc. is used. Firstly, a layer of SiO_2 is deposited on the HEMT by plasma-enhanced chemical vapor deposition (PECVD) as the HEMT selective etching mask and SAR mask. In order to make the growth window as large as possible, only the area for HEMT fabrication is protected by the SiO_2, while the other regions are etched to the i-GaN layer for SAR by dry etching with Cl_2 and BCl_3 plasma. As is shown in Fig. 2(a), for an 80 µm × 80 µm pixel, the SAR mask area is 25 µm × 50 µm, and the window ratio is 80%. After careful cleaning in piranha solution and rinsing in DI water, the selectively etched HEMT wafer is loaded into the metal-organic chemical vapor deposition (MOCVD) chamber for selective regrowth. Typical GaN-based LED growth conditions are used for µLED regrowth. The regrown µLED consists of an n-GaN layer, strain compensation shallow wells, five pairs of blue quantum wells, an AlGaN electron blocking layer, and a p-GaN layer in sequence. With a relatively large regrowth window ratio, due to the consumption of most sources in the regrowth window, the impact of the LVD of the accumulated source materials above the SiO_2 can be reduced. For the MMR process, A. Tanaka et al. reported that due to the short diffusion length L_m of Ga adatoms, if the width of the regrowth window is greater than $2L_m$, Ga adatoms at the edge of the window will not reach the center, which will lead to the formation of a thicker epitaxial layer at the edge [21]. A. Tanaka et al. showed an extracted Ga adatom diffusion length of 29-35 µm. The SAR mask in this work has a width of 25 µm and an opening width of 55 µm along $[1\bar{1}00]$. The opening width is less than $2L_m$. Therefore, the effect of the MMR on the thickness variation could be weakened. In addition, to eliminate the influence of lateral overgrowth, $(1\bar{1}00)$ facet is chosen as the interface for HEMT and regrown µLED. It has been reported that lateral growth is anisotropic, and the lateral growth rate decreases with the orientation changing from $[11\bar{2}0]$ to $[1\bar{1}00]$ [23]. This is because the lateral growth along $[1\bar{1}00]$ always features a $(1\bar{1}01)$ slant sidewall, while $(1\bar{1}01)$ has a slow growth rate because it is the most stable facet of GaN [23,24]. Figure 2(b) shows the cross-sectional SEM image of $(11\bar{2}0)$ plane at the joint position of HEMT and µLED. The SEM image shows clearly that the angle between the slant plane and (0001) is 62°, indicating a $(1\bar{1}01)$ sidewall leading to the suppression of lateral overgrowth. No apparent lateral overgrowth can be observed, and the regrown µLED is seamlessly connected with HEMT.

After the selective regrowth, the SiO_2 mask was entirely removed by the BOE solution. Subsequently, the active regions of the µLED-HEMT pixels were protected by the SiO_2 hard mask, while the redundant regrown LED was etched away by BCl_3 and Cl_2-based ICP dry etching for pixel isolation as shown in Fig. 2(a). Afterward, 30 minutes of chemical treatment in 85°C tetramethylammonium hydroxide (TMAH) solution was applied to smoothen the sidewall and repair the etching damages. HEMT source ohmic contact, LED current spreading layer (CSL), and HEMT gate metal were formed by the e-beam evaporator in the sequence of annealing temperature from high to low. When the metal contacts were complete, the whole surface was passivated by a layer of 50 nm Al_2O_3 deposited by atomic layer deposition, with all electrode contact holes opened by BOE. Subsequently, the metal stack of Ti/Al/Ti/Au (20/200/50/50 nm) was deposited by the e-beam evaporator to connect each column's source/gate electrodes and p-electrodes of each row. The isolation and planarization are achieved by spin coating a layer

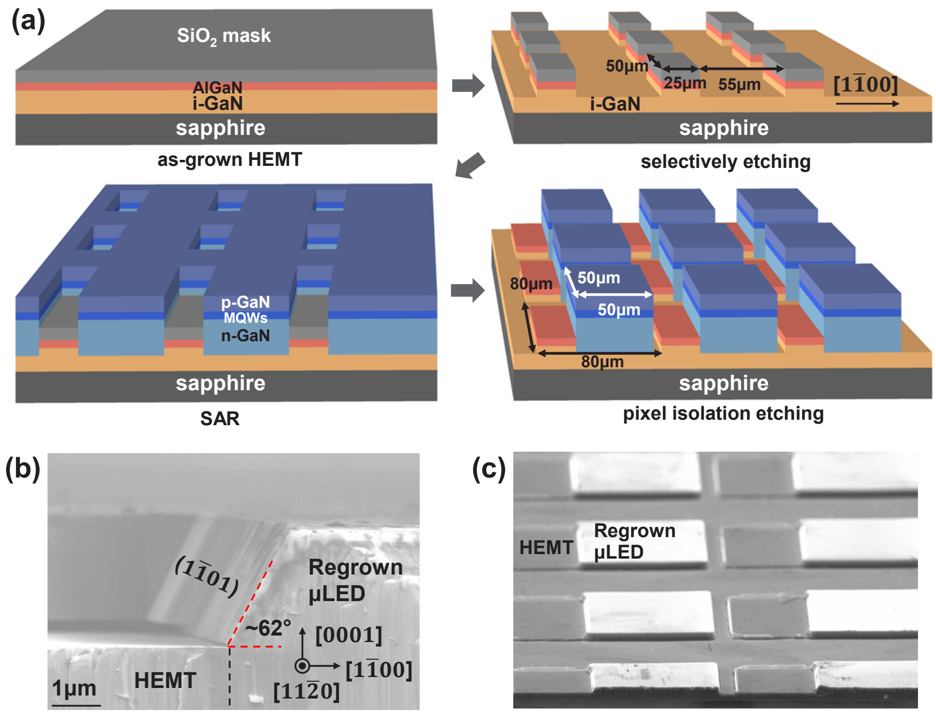

Fig. 2. (a) Schematic diagram of selective area regrowth process for monolithic integrated μLED-HEMT display, and (b) cross-sectional SEM image of (11$\bar{2}$0) after SAR and (c) SEM image after pixel isolation etch

of EOC, a commercial transparent negative photoresist. As shown in Fig. 1(a), the source/gate bus line is located at the lower part, and the p-electrodes bus lines are at the top side. When all fabrication processes were complete, μLED-HEMT arrays were laser-diced, and Al-wire bonded on the PCB driver.

3. Results and discussion

The monolithic integrated μLED-HEMT is equivalent to a depletion mode HEMT and a μLED connected in series. HEMT provides the driving current for μLED emission and could modulate luminance by tuning the gate voltage, leading to depleting and forming of 2DEG. Figure 3(a) shows the dual sweep transfer curves of the μLED-HEMT at $V_{DS} = 10$ V. A threshold voltage V_{TH} of -3.9 V is defined at $I_D = 0.01$ mA/mm. Since a current of only several microamperes is enough to light up the μLED, the off-state current of the μLED-HEMT becomes a crucial parameter for the complete turn-off of the μLED. The off-state current is ~10 nA, indicating the capability of the complete turn-off of the 50 μm μLED by depleting the 2DEG. Figure 3(b) shows the output characteristic with V_G varying from 1 V to -5 V with a step of -1 V. Compared with the conventional HEMT, the output curve of the μLED-HEMT has a right shift, which is attributed to the turn-on voltage dropped on the μLED. Regarding the on-state performance, the μLED-HEMT device can achieve a maximum driving current density of 690.4 A/cm^2 for μLED at $V_{GS} = 1$ V and $V_{DS} = 10$ V, which is adequate to drive the μLED for display.

Figure 4(a) shows the EL spectra measured in the integrating sphere with an increased current density. The EL spectra show a peak wavelength of around 456 nm. Figure 4(b) plots the peak EL wavelength and FWHM as a function of injection current density. The peak EL wavelength decreases with increasing current density until 400 A/cm^2. As the current density increases

Optics EXPRESS

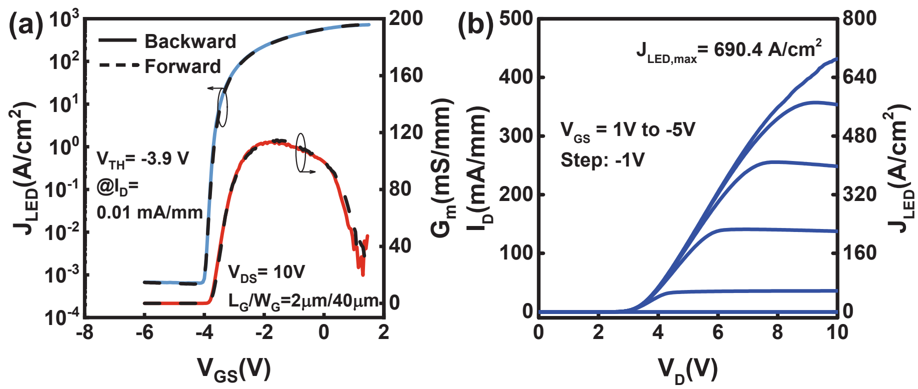

Fig. 3. (a) Transfer and (b) output characteristics of the μLED-HEMT

further, the peak wavelength starts to rise. The blueshift of peak wavelength could be attributed to the screen of the quantum confinement stack effect and band-filling effect, while the redshift of peak wavelength at high current densities results from bandgap shrinkage with increased junction temperature [25,26]. The monotonic increase of full-width half maximum (FWHM) from 27 to 32 nm could originate from the band-filling effect [27]. Figure 4(c) and (d) plot the LOP, EQE, and effective EQE (EEQE) of the μLED-HEMT. The results have also been compared with similar integrated devices [9,10,14,15,28]. Table 1 gives the devices' dimensions and the integration methods for comparison. The μLED-HEMT shows a maximum LOP of 36.2 W/cm^2 at 625 A/cm^2 and a peak EQE of 3.36% at 45.6 A/cm^2, respectively. The EEQE is defined by Eq. (1) [9,14],

$$EEQE = \frac{LOP}{I \cdot V_D} \tag{1}$$

$$\begin{aligned} V_D &= I \cdot R_{\mu LED-HEMT} \\ &= I \cdot (R_{\mu LED} + R_{HEMT} + R_i) \end{aligned} \tag{2}$$

where I is the current that passes through the μLED-HEMT, V_D is the voltage drops on the device, and it can be expressed by Eq. (2), where $R_{\mu LED}$, $R_{HEMT,}$ and R_i represents the resistance of μLED, HEMT, and interconnection resistance, respectively. The μLED-HEMT shows a peak EEQE of 2.59% at 29.7 A/cm^2. When comparing the results with similar integrated devices, the μLED-HEMT shows a higher LOP and EEQE at the correspondent current density with a smaller device dimension. It is well known that the optical performance of the μLED decreases with the decreased device size due to a larger surface-to-volume ratio, leading to a more significant effect of non-radiation recombination centers by surface defects on device performance [29,30]. Therefore, the improved optical performance indicates an improved crystal quality of the regrown μLED with a large SAR window ratio and effective passivation of the μLED-HEMT than other reported works. In addition to the increased LOP, the improvement of EEQE could also be attributed to the lower R_{HEMT} of HEMT compared to GaN MOSFETs and nanowire FETs, as well as the reduced R_i by this metal interconnection-free integration scheme.

In addition, the μLED-HEMT array with a display result is demonstrated. Figure 5(a) plots the transfer curve of forty μLED-HEMT pixels from the display with the error band, showing the mean and the standard deviation, and Fig. 5(b) shows the statistical results of the on-state performance at $V_D = 7$ V. The variation between the pixels could be ascribed to the nonuniformity problem in the growth and fabrication process. Figure 5(c) shows the photograph of the μLED-HEMT display system. Selective emission of the pixels is achieved by receiving signals from FPGA. FPGA reads the binary data from the SD memory card when the system is powered up, generating

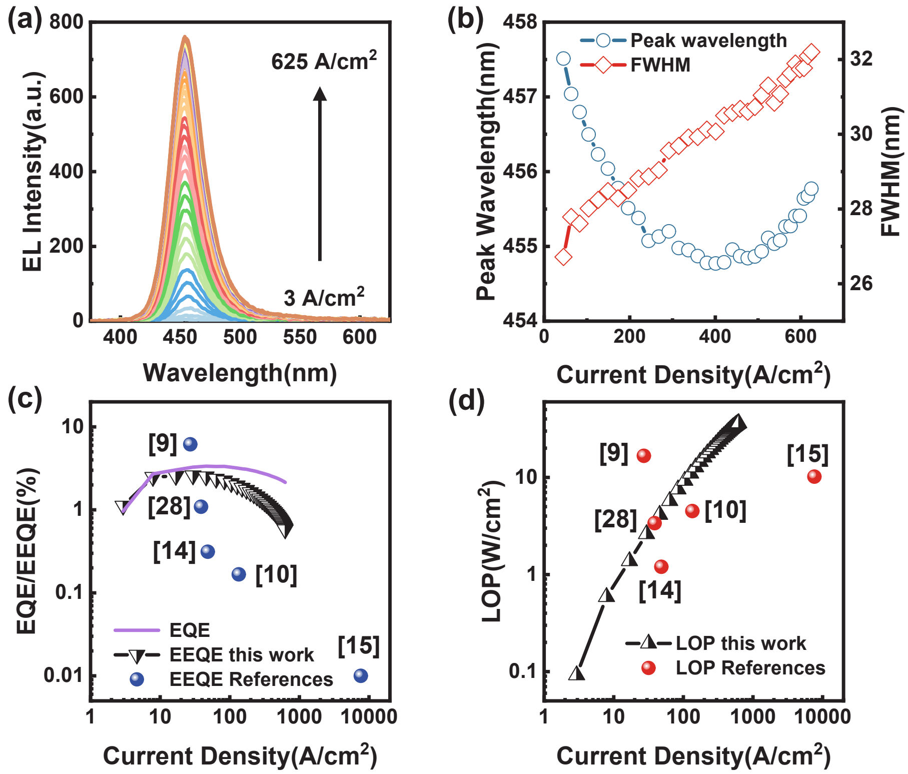

Fig. 4. (a) EL spectra, and (b) peak wavelength and FWHM at different current densities. (c) EQE, EEQE, and (d) LOP of the μLED-HEMT and reference works

Table 1. Summary of monolithic integrated GaN-based LED and transistors[a]

Ref. No.	Device dimension (μm^2)	Driving transistor	Method	I/V	LOP
[9]	800 × 600	HEMT	SER	130 mA/10V	80mW
[10]	100 × 100	MOSFET	SER	13.5 mA/20V	0.45mW
[14]	450 × 460	HEMT	SAR	100 mA/8V	2.5mW
[15]	D = 20	HEMT	SAR	24 mA/12V	32μW
[28]	450 × 460	HEMT	SAR	80 mA/8V	7mW
This work	50 × 50	HEMT	SAR	15.6 mA/10V	0.9mW

[a]SER: selective epitaxial removal

the scan and data signal to the μLED-HEMT array. Figure 5(d) shows the photographs of the μLED-HEMT display showing the “HKUST”. The display is not very good, which might be limited by the low yield and optical crosstalk issue. It is believed that the display could be improved with a further optimized growth condition and fabrication process. Furthermore, with a proper design, monolithic integration of enhancement-mode HEMT-based 2T1C and μLED can be achieved by SAR, achieving an active-matrix μLED display and further improving the quality and efficiency of the display.

Optics EXPRESS

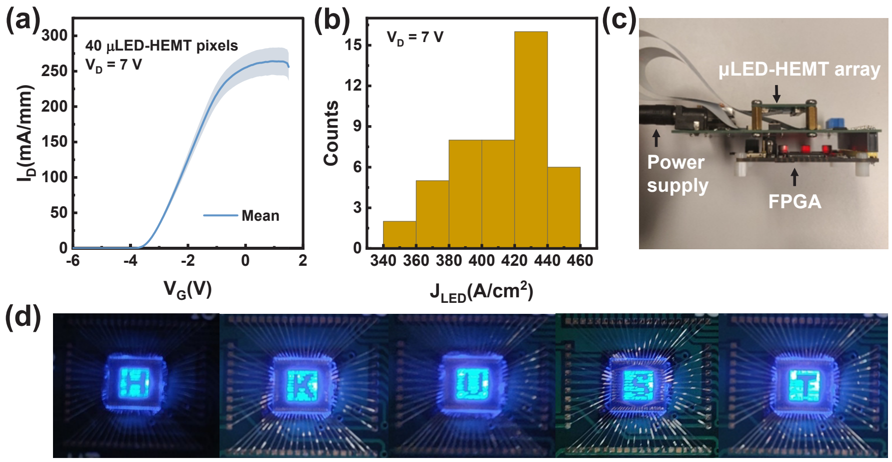

Fig. 5. (a) Transfer curve and (b) statistic on-state performance of 40 μLED-HEMT pixels. (c) photographs of the μLED-HEMT display system and (d) showing "HKUST"

4. Conclusion

In summary, this work demonstrates a monolithic integrated 20×20 μLED-HEMT display by the SAR method. By designing a SAR pattern with a large regrowth window ratio and surface treatment, the μLED-HEMT device shows improved optical performance. The μLED-HEMT has a LOP of 36.2 W/cm^2 and a peak EQE of 3.36%. Letters of "HKUST" are successfully displayed on the μLED-HEMT display system with a customized driving PCB. Although the display is not very satisfactory at the current stage, this work has provided a practical, process-compatible, and flip-chip-bonding-free approach for a homogenous integrated μLED display. It also suggests the potential of achieving a monolithic integrated all-GaN-based active-matrix μLED display.

Funding. Shenzhen Science and Technology Program (JCYJ20220818100603007); Fundamental and Applied Fundamental Research Fund of Guangdong Province (2021B1515130001).

Acknowledgments. The authors would like to thank the Nanosystem Fabrication Facility (NFF) of HKUST for their technical support. The authors would also like to thank Chak Wah Tang for his help in the MOCVD regrowth process. Helpful discussions with Fulong Jiang and Byung-Ryool Hyun are also acknowledged.

Disclosures. The authors declare no conflicts of interest.

Data availability. Data underlying the results presented in this paper are not publicly available at this time but may be obtained from the authors upon reasonable request.

References

1. J. Lin and H. Jiang, "Development of microLED," Appl. Phys. Lett. **116**(10), 100502 (2020).
2. T. Jung, J. H. Choi, S. H. Jang, and S. J. Han, "Review of Micro-light-emitting-diode Technology for Micro-display Applications," SID Symp. Digest of Technical Papers **50**(1), 442–446 (2019).
3. Y. Huang, E.-L. Hsiang, M.-Y. Deng, and S.-T. Wu, "Mini-LED, Micro-LED and OLED displays: Present status and future perspectives," Light: Sci. Appl. **9**(1), 105 (2020).
4. P. J. Parbrook, B. Corbett, J. Han, T. Y. Seong, and H. Amano, "Micro-Light Emitting Diode: From Chips to Applications," Laser Photonics Rev. **15**(5), 2000133 (2021).
5. A. Xz, A. Pt, B. Cws, W. C. Jiang, C. Hl, L. A. Ran, and B. J. P. i. Q. E. Hck, "Growth, transfer printing and colour conversion techniques towards full-colour micro-LED display," Prog. Quantum. Electron. **71**, 100263 (2020).
6. Z. Lei, O. Fang, W. C. Chong, Y. Chen, and Q. J. J. O. T. S. F. I. D. Li, "Wafer-scale monolithic hybrid integration of Si-based IC and III–V epi-layers—A mass manufacturable approach for active matrix micro-LED micro-displays," J. Soc. Inf Disp. **26**(3), 137–145 (2018).
7. S. Bharadwaj, K. Lee, K. Nomoto, A. Hickman, L. van Deurzen, V. Protasenko, H. Xing, and D. Jena, "Bottom tunnel junction blue light-emitting field-effect transistors," Appl. Phys. Lett. **117**(3), 031107 (2020).
8. Y. Cai, X. Zou, C. Liu, and K. M. Lau, "Voltage-controlled GaN HEMT-LED devices as fast-switching and dimmable light emitters," IEEE Electron Device Lett. **39**(2), 224–227 (2018).

Optics EXPRESS

9. D. Chen, Z. Liu, X. Lu, L. Wan, R. Li, Z. Yang, and G. Li, "Efficiency improved by monolithic integration of HEMT with vertical-structure LEDs and Mg doping on dry etched GaN," J. Mater. Chem. C **7**(10), 2823–2828 (2019).
10. Z. Guo, C. Hitchcock, C. Wetzel, R. F. Karlicek, G. Piao, Y. Yano, S. Koseki, T. Tabuchi, K. Matsumoto, and M. Bulsara, "Monolithically Integrated GaN LED/Quasi-Vertical Power U-Shaped Trench-Gate MOSFET Pairs Using Selective Epi Removal," IEEE Electron Device Lett. **40**(11), 1736–1739 (2019).
11. M. Hartensveld and J. Zhang, "Monolithic Integration of GaN Nanowire Light-Emitting Diode With Field Effect Transistor," IEEE Electron Device Lett. **40**(3), 427–430 (2019).
12. R. Gaska, J. Yang, A. Osinsky, Q. Chen, M. A. Khan, A. Orlov, G. Snider, and M. Shur, "Electron transport in AlGaN–GaN heterostructures grown on 6H–SiC substrates," Appl. Phys. Lett. **72**(6), 707–709 (1998).
13. Z. Lei, M. Xu, X. H. Xia, J. H. Zou, L. R. Zhang, D. X. Luo, W. J. Wu, L. Wang, and J. B. Peng, "Power consumption model for AMOLED display panel based on 2T-1C pixel circuit," J. Display Technol. **12**(10), 1064–1069 (2017).
14. C. Liu, Y. Cai, Z. Liu, J. Ma, and K. M. Lau, "Metal-interconnection-free integration of InGaN/GaN light emitting diodes with AlGaN/GaN high electron mobility transistors," Appl. Phys. Lett. **106**(18), 181110 (2015).
15. Y. Cai, C. Zhu, W. Zhong, P. Feng, S. Jiang, and T. J. A. M. T. Wang, "Monolithically Integrated μLEDs/HEMTs Microdisplay on a Single Chip by a Direct Epitaxial Approach," Adv. Mater. Technol. **6**(6), 2100214 (2021).
16. Y. Sakata, Y. Inomoto, and K. Komatsu, "Surface migration effect and lateral vapor-phase diffusion effect for InGaAsP/InP narrow-stripe selective metal-organic vapor-phase epitaxy," J. Cryst. Growth **208**(1-4), 130–136 (2000).
17. Y. Tomita, T. Shioda, M. Sugiyama, Y. Shimogaki, and Y. Nakano, "Role of vapor-phase diffusion in selective-area MOVPE of InGaN/GaN MQWs," J. Cryst. Growth **311**(10), 2813–2816 (2009).
18. D. Kapolnek, S. Keller, R. Vetury, R. Underwood, P. Kozodoy, S. Den Baars, and U. Mishra, "Anisotropic epitaxial lateral growth in GaN selective area epitaxy," Appl. Phys. Lett. **71**(9), 1204–1206 (1997).
19. F. Yang, Y. Yao, Z. Y. He, G. L. Zhou, Y. Zheng, L. He, J. C. Zhang, Y. Q. Ni, D. Q. Zhou, Z. Shen, J. Zhong, Z. S. Wu, B. J. Zhang, and Y. Liu, "The suppression of background doping in selective area growth technique for high performance normally-off AlGaN/GaN MOSFET," J. Mater. Sci.: Mater. Electron. **26**(12), 9753–9758 (2015).
20. K. C. Zeng, J. Y. Lin, H. X. Jiang, and W. Yang, "Optical properties of GaN pyramids," Appl. Phys. Lett. **74**(9), 1227–1229 (1999).
21. A. Tanaka, R. Chen, K. L. Jungjohann, and S. A. Dayeh, "Strong geometrical effects in submillimeter selective area growth and light extraction of GaN light emitting diodes on sapphire," Sci. Rep. **5**(1), 17314 (2015).
22. M. Ueda, T. Kondou, K. Hayashi, M. Funato, Y. Kawakami, Y. Narukawa, and T. Mukai, "Additive color mixture of emission from InGaN/GaN quantum wells on structure-controlled GaN microfacets," Appl. Phys. Lett. **90**(17), 171907 (2007).
23. I. Mahaboob, J. Marini, K. Hogan, E. Rocco, R. P. Tompkins, N. Lazarus, and F. Shahedipour-Sandvik, "Selective area epitaxial growth of stretchable geometry AlGaN-GaN heterostructures," J. Electron. Mater. **47**(11), 6625–6634 (2018).
24. J. Park, P. Grudowski, C. Eiting, and R. Dupuis, "Selective-area and lateral epitaxial overgrowth of III–N materials by metal organic chemical vapor deposition," Appl. Phys. Lett. **73**(3), 333–335 (1998).
25. T. Takeuchi, S. Sota, M. Katsuragawa, M. Komori, H. Takeuchi, H. A. H. Amano, and I. A. I. Akasaki, "Quantum-confined Stark effect due to piezoelectric fields in GaInN strained quantum wells," Jpn. J. Appl. Phys. **36**(4A), L382 (1997).
26. W.-C. Ke, F.-W. Lee, C.-Y. Chiang, Z.-Y. Liang, W.-K. Chen, and T.-Y. Seong, "InGaN-based light-emitting diodes grown on a micro/nanoscale hybrid patterned sapphire substrate," ACS Appl. Mater. Interfaces **8**(50), 34520–34529 (2016).
27. Y.-J. Lee, C.-H. Chiu, C. C. Ke, P. C. Lin, T.-C. Lu, H.-C. Kuo, and S.-C. Wang, "Study of the excitation power dependent internal quantum efficiency in InGaN/GaN LEDs grown on patterned sapphire substrate," IEEE J. Sel. Top. Quantum Electron. **15**(4), 1137–1143 (2009).
28. C. Liu, Y. Cai, X. Zou, and K. M. Lau, "Low-leakage high-breakdown laterally integrated HEMT-LED via n-GaN electrode," IEEE Photonics Technol. Lett. **28**(10), 1130–1133 (2016).
29. A. Daami, F. Olivier, L. Dupré, F. Henry, and F. Templier, "Electro-optical size-dependence investigation in GaN micro-LED devices," SID Symp. Digest of Technical Papers **49**(1), 790–793 (2018).
30. J. M. Smith, R. Ley, M. S. Wong, Y. H. Baek, J. H. Kang, C. H. Kim, M. J. Gordon, S. Nakamura, J. S. Speck, and S. P. DenBaars, "Comparison of size-dependent characteristics of blue and green InGaN microLEDs down to 1 μm in diameter," Appl. Phys. Lett. **116**(7), 071102 (2020).